JGR Oceans

RESEARCH ARTICLE
10.1029/2025JC022577

Meso- and Submesoscale Circulation Origins for Subsurface Oxygen Intrusions Into the Oxygen Deficient Zone of the Eastern Tropical North Pacific

A. Pietri[1,2], **M. Altabet**[1], **G. W. Cowles**[1], **and E. D'Asaro**[3]

[1]School for Marine Science and Technology, University of Massachusetts Dartmouth, New Bedford, MA, USA, [2]Now at LOCEAN-IPSL, Sorbonne Université, IRD, CNRS, MNHN, Paris, France, [3]Applied Physics Laboratory, University of Washington, Seattle, WA, USA

Key Points:

- The eastern tropical North Pacific oxygenated deficient zone is ventilated at depth by waters traveling from the coast
- Gap winds in the Gulfs of Papagayo and Tehuantepec can form eddies and filaments advecting high chlorophyll and high oxygen water offshore

Correspondence to:
A. Pietri,
alice.pietri@ird.fr

Citation:
Pietri, A., Altabet, M., Cowles, G. W., & D'Asaro, E. (2025). Meso- and submesoscale circulation origins for subsurface oxygen intrusions into the oxygen deficient zone of the eastern tropical North Pacific. *Journal of Geophysical Research: Oceans*, *130*, e2025JC022577. https://doi.org/10.1029/2025JC022577

Received 2 MAR 2025
Accepted 18 JUL 2025

Author Contributions:
Conceptualization: A. Pietri, M. Altabet
Formal analysis: A. Pietri, M. Altabet, E. D'Asaro
Funding acquisition: M. Altabet, E. D'Asaro
Methodology: A. Pietri, M. Altabet, G. W. Cowles
Project administration: M. Altabet
Visualization: A. Pietri
Writing – original draft: A. Pietri
Writing – review & editing: M. Altabet, G. W. Cowles, E. D'Asaro

Abstract Subsurface oxygen maxima (SOM) are recurrent but poorly understood features within the eastern tropical North Pacific oxygen deficient zone (ODZ). Here, we analyze a subsurface oxygen maximum (SOM) observed during the SR2114 cruise using in situ biogeochemical and physical measurements, satellite remote sensing, and Lagrangian particle tracking. The SOM was detected around the 26.4 isopycnal (~150–200 m) and spatially associated with elevated oxygen concentrations within an otherwise hypoxic environment. Our results show that intense gap winds in the Gulfs of Tehuantepec and Papagayo generate strong upwelling, vertical mixing, and horizontal advection near the coast, potentially allowing subsurface layers to come into contact with surface waters and become oxygenated. The observed vertical penetration of wind-driven features below the Ekman layer also suggests the influence of eddy-wind interactions that reinforce vertical coherence and enhance the offshore transport of oxygen-rich waters. The offshoreward jets observed down to the SOM layer depth highlight the contribution of such coupled processes to ventilating the ODZ interior. Furthermore, float-based observations along isopycnals indicate progressive oxygen loss over time, likely due to local respiration, pointing to dynamic interplay between physical supply and biogeochemical consumption. Together, these findings underscore the pivotal role of coastal wind forcing and mesoscale dynamics in shaping the subsurface oxygen landscape of the eastern tropical North Pacific. The Lagrangian analysis also highlights distinct pathways for water parcels within the ODZ: south of 14°N, water masses are primarily influenced by equatorial currents, whereas in the northern region, water parcels predominantly originate from coastal sources with extended residency times.

Plain Language Summary The eastern tropical North Pacific (ETNP) is home to one of the largest regions of severely low oxygen in the ocean, an oxygen deficient zone (ODZ). While researchers have learned a lot about the physical and biogeochemical processes that control oxygen concentration in these areas, some key details remain unclear. This study explores the origin and movement of a patch of relatively oxygen-enriched water, known as a subsurface oxygen maximum (SOM), found at depths of 150–250 m within the low-oxygen core of the ETNP. Using direct measurements from the ocean, satellite observations, and particle tracking tools, the research shows that these oxygenated waters likely come from coastal areas, particularly near the Gulf of Tehuantepec. In this region, strong winds drive upwelling (where deeper water rises to the surface) and horizontal movements that create dynamic filaments and eddies, transporting oxygen-enriched waters offshore. These physical processes, combined with biological activity, shape the distribution of oxygen in the ODZ. Still, many small-scale processes and biological interactions remain uncertain, leaving gaps in understanding how oxygen spreads and is consumed in the ODZ. This knowledge is critical for predicting how these low-oxygen areas may respond to climate change and their potential effects on marine ecosystems.

1. Introduction

Oxygen deficient zones (ODZs) are characterized by very low to undetectable oxygen concentrations within the water column and play a crucial role in a range of marine biogeochemical processes. ODZs occur due to a combination of factors, including high surface productivity, weak ventilation, and stratification (Engel et al., 2022; Oschlies et al., 2018). The availability of dissolved oxygen (O_2) is a key metabolic constraint for marine ecosystems, exerting a profound influence on the habitat preferences of aerobic organisms while favoring anaerobic microbial metabolisms.

ODZs, typically defined by oxygen levels below 60 μmol L^{-1} can range from hypoxic (5–60 μmol L^{-1}), to suboxic (<5 μmol L^{-1}), and to anoxic (0 μmol L^{-1}) conditions (Engels et al., 2022). They are found in all of the world's oceans but are most extensive in the tropical and subtropical Pacific Ocean, with the largest in the eastern tropical North Pacific (ETNP, Kwiecinski & Babbin, 2021). These regions play a significant role in the global nitrogen cycle, carbon sequestration, and the production of greenhouse gases. Denitrification and anammox, major microbial sinks for biologically available nitrogen, occur in ODZs and regulate the global amount available for phytoplankton growth. Additionally, microbes in ODZs also produce nitrous oxide and methane, greenhouse gases that could contribute to climate change. ODZs also have significant ecological implications. Many marine organisms including those of economic importance cannot survive in these low-oxygen environments, leading to changes in the distribution and abundance of marine life around ODZs (Fiedler et al., 2013). Understanding the dynamics of these zones is therefore critical for predicting their impact on marine ecosystems and biogeochemical cycles.

However, despite the general understanding that ODZs exist due to a balance between oxygen supply and consumption, current models struggle to accurately reproduce them or the observed trends of deoxygenation (Schmidtko et al., 2017). One of the main difficulties lies in resolving processes at small spatiotemporal scales (Duteil et al., 2014). The importance of mesoscale and submesoscale processes, such as eddies and filaments, in shaping the distribution and transport of oxygen and other biogeochemical properties in the ocean has been increasingly recognized (Lévy et al., 2018; Nagai et al., 2015). These processes play a critical role in the lateral and vertical redistribution of water masses, particularly in regions with complex circulation patterns like the ETNP. However, the full extent of their influence remains difficult to quantify due to the limitations in observational coverage and the challenges of capturing fine-scale dynamics over large spatial and temporal scales. In fact, while ODZs are predominantly ventilated across their open-ocean boundaries, meso- and submesoscale processes at the coast could also play a crucial role in the subduction and advection of relatively oxygenated waters into the ODZs (Margolskee et al., 2019). This emphasizes the need for more detailed observations and analyses to improve our understanding of these coastal processes and their contribution to ODZ ventilation and the corresponding model predictions.

In this paper, we present observations in the coastal region of the ETNP and the corresponding ODZ. The circulation in the region is shaped by a combination of large-scale currents, mesoscale features, and wind-driven processes. The region is influenced by the North Pacific gyre to the north and the equatorial current system to the south, with the North Equatorial Current and the North Equatorial Countercurrent (NECC) driving the east-west water transport. Coastal currents, such as the Costa Rica Coastal Current, further contribute to alongshore and cross-shore exchanges (Kessler, 2006). Eddies and filaments are common mesoscale features in the ETNP (Hasson et al., 2019; Willet et al., 2006), arising from wind forcing, coastal processes, and instabilities in the larger circulation. These structures enhance horizontal and vertical transport, influencing the distribution of nutrients, heat, and biogeochemical properties.

The observations presented here from various sources allow us to investigate the patchy distribution in time and space of a subsurface oxygen maximum (SOM) within the ETNP ODZ. This SOM is wrapped around eddies that form at the coast and are advected westward inside the ODZ. We argue that this SOM plays an important role in the ventilation of the ODZ by transporting oxygen from coastal regions into the core of the ODZ. By combining physical and biogeochemical in situ data with satellite information for sea level anomaly (SLA), finite-size Lyapunov exponents (FSLE), chlorophyll a (chl-a), and wind patterns, we aim to elucidate the mechanisms driving the distribution of oxygen and other key properties within the ODZ. Through Lagrangian particle tracking analysis with satellite-derived surface currents and modeled subsurface currents, we gain valuable insights into the origins of the observed SOM. This comprehensive approach sheds light into the complex interactions between physical and biogeochemical processes in this critical region of the world's oceans.

2. Data and Methods

2.1. Data

The SR2114 cruise was conducted between December 2021 and January 2022 off the coast of Central America aboard the RV Sally Ride. A rosette equipped with a conductivity-temperature-depth (CTD) probe and a sensor to measure dissolved oxygen (SBE-43) recorded 97 vertical profiles at 51 station locations. To reference the SBE-43 data to anoxia (±50 nM) in the core waters of the ODZ a switchable trace amount oxygen sensor (Revsbech

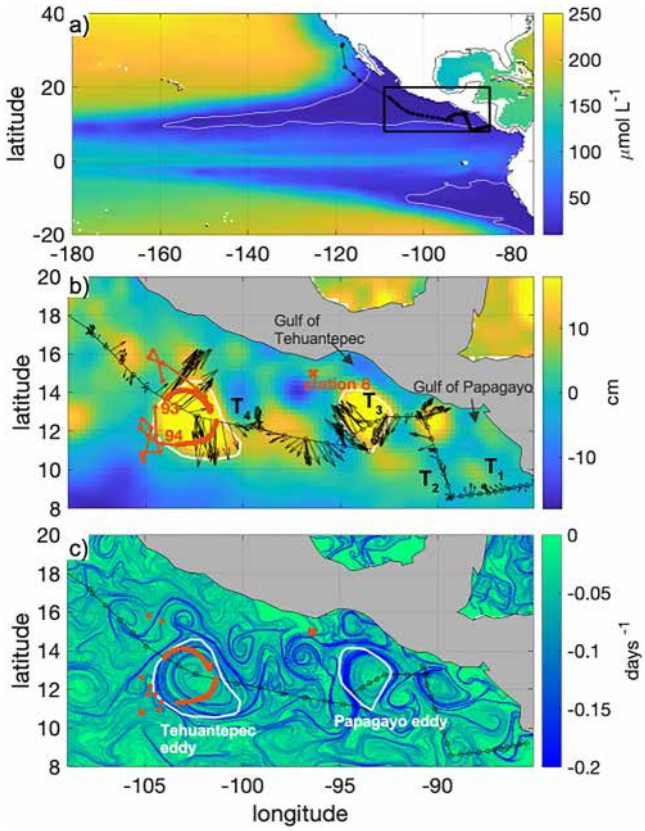

Figure 1. (a) Climatology of dissolved oxygen concentration from Roach and Bindoff (2023, μmol L^{-1}) at 200 m depth over the tropical Pacific. The white contour corresponds to a concentration of 20 μmol L^{-1}. The black rectangle indicates the region highlighted on the following maps. Satellite (b) sea level anomaly and (c) finite-size Lyapunov exponents on 10 January 2022. The ship's track is indicated by a black line with the stations highlighted by black circles, and the arrows on panel (a) represent the depth averaged (0–100 m) acoustic doppler current profilers velocity. The white lines represent the edges of the two eddies as provided by the mesoscale eddy trajectories atlas. In orange are the floats trajectories and the coastal station 8 sampled on 14 February 2023. The ship's transects are indicated as $T_{1\text{-}4}$.

et al., 2011) was used to recalibrate the data (McNeil et al., 2023). The campaign consisted of four transects, two around the Costa Rica Dome (CRD) and the Gulf of Papagayo (transects 1 and 2), one extending offshore of Guatemala south of the Gulf of Tehuantepec (transect 3) and one traveling northward parallel to the coast of Mexico (transect 4, Figure 1a). During the cruise, direct measurements of horizontal current were recorded using vessel-mounted acoustic doppler current profilers (ADCP) at 38 and 300 kHz. The ADCP data were processed using the Common Ocean Data Access System software, developed and maintained by the University of Hawaii, which allows corrections for ship motion and averaging over specified intervals (Firing et al., 1995). The 38 kHz device recorded velocity from 44 to 1,820 m depth at a vertical resolution of 24 m while the 300 kHz ADCP reached a vertical resolution of 2 m between 10 and 108 m depth.

As SR2114 did not sample along the western Mexico coast, we took advantage of data available from a subsequent cruise of the RV Atlantis II to explore the Gulf of Tehuantepec as a source region of the SOM. Station 8 of AT5008 (Figure 1) was occupied on 14 February 2023, and we report here the profile of O_2.

During the campaign, several floats were deployed. These included two floats developed by marine robotics systems (MRV) and modified to carry optode oxygen sensors in addition to the standard temperature, salinity, and depth measurements. The MRV floats were both deployed around an anticyclonic eddy during the fourth transect along the coast of Mexico (Figure 1).

Several satellite-derived data sets were used to contextualize in situ data and provide information on the surface ocean dynamics. The delayed-time "all-sat" SLA product from the Archiving, Validation, and Interpretation of Satellite Oceanographic (AVISO) service, and distributed by the Copernicus Marine Environment Monitoring Service (CMEMS), consists of global daily gridded SLA observations at a resolution of 0.25°. Surface geostrophic velocities, derived from the slope of the sea surface height are also provided and were used in the present work to study transport mechanisms.

Additionally, we use FSLE, a diagnostic tool used to quantify the rate at which initially close pairs of particles diverge over time, providing a Lagrangian measure of stretching and mixing. High FSLE values typically identify transport barriers or fronts, along which biogeochemical tracer distribution tend to organize. FSLE intensities are calculated based on the method of d'Ovidio et al. (2004) and provided at a spatial resolution of 0.04° by AVISO. To further explore the mesoscale structures, we employed the altimetric mesoscale eddy trajectories atlas (META3.2 DT) produced by SSALTO/DUACS and distributed by AVISO+ (https://aviso.altimetry.fr) with support from CNES, in collaboration with IMEDEA (https://agupubs.onlinelibrary.wiley.com/doi/full/10.1029/2025JC022518). It provides location, contours, amplitude, radius, and speed for anticyclonic and cyclonic eddies detected from the multimission altimetry data sets (Pegliasco et al., 2022).

Chlorophyll a (chl-a) concentration data were sourced from the CMEMS. The specific product used in this study is the Chl-a concentration in seawater derived from satellite observations of ocean color sensors and provided on a daily grid with a spatial resolution of approximately 1 km.

To assess the wind forcing we use the global ocean daily gridded sea surface winds at 0.25° resolution from available scatterometers distributed by CMEMS. We consider the 10-m wind components as well as the wind stress. Using these data, the Ekman transport components (U_{ek}, V_{ek}) are calculated in the area of the Gulf of Tehuantepec in the following way:

$$U_{ek} = \frac{\tau_0{}^y}{\rho_0 f}, V_{ek} = \frac{-\tau_0{}^x}{\rho_0 f}$$

where $\tau_0{}^x$ and $\tau_0{}^y$ are the eastward and northward components of the wind stress, respectively; ρ_0 a reference density for seawater in the region; and f the Coriolis parameter. Finally the Ekman pumping, w_{ek}, which correspond to the vertical velocity at the base of the Ekman layer driven by the wind stress curl, was also estimated as follows:

$$w_{ek} = \frac{1}{\rho_0 f}\left(\frac{\partial \tau_0{}^y}{\partial x} - \frac{\partial \tau_0{}^x}{\partial y}\right).$$

2.2. Lagrangian Analysis of Water Parcels

To investigate the source and trajectories of relatively oxygenated water parcels observed along the cruise track and by the MRV floats, we used the parcels framework (version 3.0, Lange & van Sebille, 2017) to simulate pathways from and into the ODZ. Parcels is an open-source Python-based framework designed to conduct Lagrangian ocean experiments by tracking virtual particles through hydrodynamic fields. It is used for the mapping of pathways and connectivity of water parcels and can simulate, for example, the displacement of plankton (Dämmer et al., 2020), plastic (Duncan et al., 2018), or fish (Schilling et al., 2020). The parcels code is developed with scalability in mind and introduces interpolation schemes for reading various types of discretized fields, model-generated as well as observation-based. The full code of the tracking algorithm is available at https://oceanparcels.org/index.html.

We conducted two numerical particle tracking experiments. For the first one, we tracked particles backward in time to examine source locations of surface water along the ship track. To conduct this, particles were driven by satellite-derived surface geostrophic velocity fields at a daily time step. In the second numerical experiment, particles are transported at depth by the regional velocity field predicted by a 3D hydrodynamic circulation model. For this, we selected the HYCOM + NCODA GOFS 1/12° analysis (GLBy0.08) product, which represents a combination of the HYCOM ocean model and the NCODA data assimilation system. The hybrid isopycnal-sigma-pressure coordinate ocean model HYCOM solves the hydrostatic Navier-Stokes equations on a global domain while the NCODA variational data assimilation system integrates a variety of observational information into the HYCOM model. This GLBy0.08 product provides estimates of different oceanographic variables, including temperature, salinity, and currents. The product is available on a global grid with a resolution of 1/12°, and we use a time step of 6 hr.

3. Results

3.1. Physical and Biogeochemical Properties

Surface properties within the ETNP exhibit distinct features indicative of strong mesoscale and submesoscale activity. Sea level anomalies (Figure 1b) reveal the presence of eddies and coherent structures and, in particular, several anticyclonic eddies (SLA highs) along the ship's track (Figure 1b). FSLE high values identify Lagrangian coherent structures that delineate transport barriers and frontal boundaries; they highlight the presence of sub-mesoscale filaments, particularly evident around the periphery of eddies (Figure 1c). This methodology has proven effective in revealing meso- and submesoscale dynamical features that organize tracer distributions, such as high chlorophyll phytoplankton patches, in upwelling systems (e.g., Gangrade & Franks, 2023). This is confirmed by the distribution of high chlorophyll concentration regions on the surface that are organized in filamentary structures originating from the productive regions in the coastal Gulf of Tehuantepec and Gulf of Papagayo areas (Figure 2). Besides being shaped by the eddy activity, the chlorophyll filaments tend to originate from the Gulfs and follow the general direction of the winds that blow through mountain gaps shoreward of these Gulfs (the so-called gap winds, Barton et al., 2009).

The thermohaline distribution of properties along the ship's track between the surface and 400 m depth is displayed in Figures 3a and 3b. The signature of the CRD is evident in transects 1 and 2. It is characterized by a surface cooling, visible between days 2 and 4, driven by a prominent upwelling. As the ship travels north, the relatively warm, fresh, and well-mixed surface layer expands to greater depth, reaching 100 m. Additionally, the

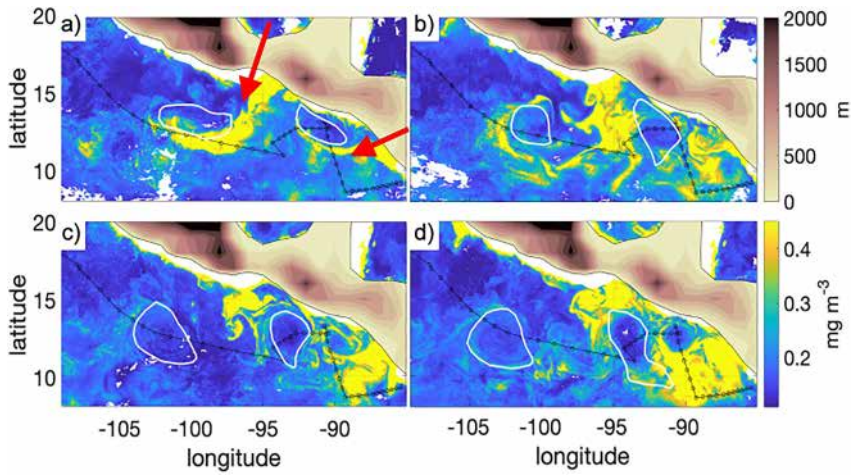

Figure 2. Satellite chlorophyll a on December 1st (a) and 15th (b) 2021 and January 1st (c) and 15th 2022 (d). The ship's track is indicated by a black line with the stations highlighted by black circles; the thin white lines represent the edges of the two eddies on the same date as the satellite image. The land topography (m) displayed in shades of brown shows the mountain range and the gaps where the wind jets (indicated by red arrows on panel a) blow.

distinctive features of two anticyclonic mesoscale eddies, the Papagayo eddy (transect 3) and the Tehuantepec eddy (transect 4), can be observed on days 7–9 and from 15 to 19: the isolines of temperature, salinity, and density deepen as the ship gets close to the center of the mesoscale structures creating horizontal gradients and a pocket of warm and fresh water isolated from the surrounding environment.

The biogeochemical properties also exhibit multiscale patterns reflective of the complex oceanic dynamics of the region (Figures 3c and 3d). The southern coastal region (days 0–8) features a higher concentration of oxygen up to 300 m depth typical of the southern boundary region of the ETNP and high surface chlorophyll fluorescence that can be attributed to CRD upwelling and enhanced biological activity. Very low (<1 μmol L^{-1}) oxygen concentrations can be observed at depth. In transects 1 and 2, the upper limit of the ODZ appears around 300 m depth; then, during transect 3, the ship is moving offshore and the upper limit of the ODZ rises to about 100 m depth. During the fourth transect, the ship is getting closer to the ODZ core; however, several occurrences of dissolved oxygen concentrations rising from several to 20 μmol L^{-1} in the 200–300 m depth range, well within the ODZ, are also observed, suggesting processes able to ventilate the ODZ. The crossing of the two eddies is characterized by a deepening of the oxycline from 50 m depth to 100 m depth for the Papagayo eddy (transect 3) and almost 200 m for the Tehuantepec eddy (transect 4). Both exhibit very low surface chlorophyll fluorescence in their centers bordered on their sides and at the bottom of their mixed layers by higher values.

Analysis of the ADCP data along the ship's track allows us to observe the horizontal circulation at the time of the cruise (Figure 4). Along the first 3 transects, the circulation is generally northward and offshore (westward) except for the eddy crossing Section 3. This is consistent with the NECC flowing east toward the coast at 5°N and then north around the CRD. Along transect 4, parallel to the coast of Mexico, the zonal circulation is mostly eastward (inshore) whereas the meridional circulation alternates between northward and southward.

At scales below the regional circulation, the flow is mainly organized around O (100 km) wide structures that are intensified at the surface but remain visible at 1,000 m depth underscoring the role of mesoscale dynamics, such as eddies and filaments, on the horizontal circulation patterns. More specifically, north of the CRD (transect 3 and 4), energetic velocities start to arise in the surface layer. The influence of the two eddies is particularly visible in the meridional flow, where a sharp transition occurs from southward to northward currents in transects 3 and 4 (days 9 and 18, Figure 4b). The first eddy exhibits an influence extending to depths exceeding 500 m while the second eddy exerts a deeper-reaching discernible influence up to 1,000 m depth.

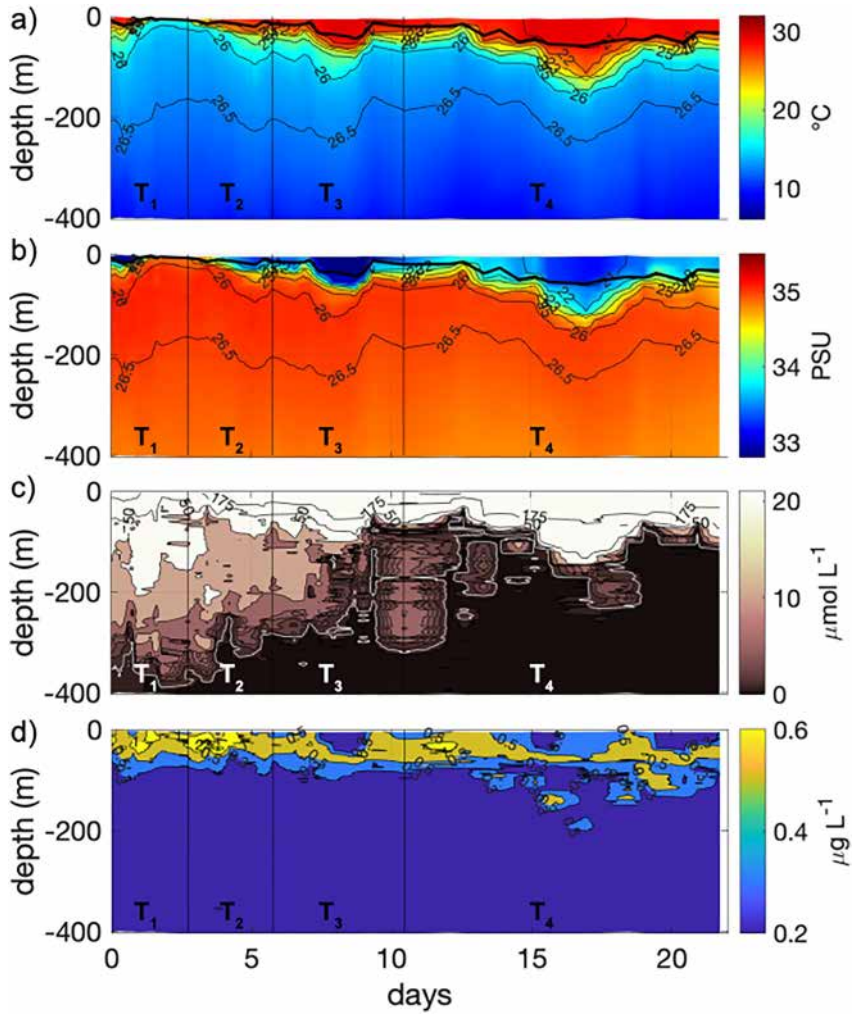

Figure 3. From top to bottom: vertical sections of (a) temperature (°C), (b) salinity (PSU), (c) oxygen (μmol L^{-1}) and (d) chl fluorescence (μg L^{-1}) interpolated between the ship's stations. Days are counted from 23 December 2021. Isopycnal contours (σ_θ) are included in black in the upper two panels (a) and (b) as well as the mixed layer depth, in bold, defined as the depth at which the temperature is 0.5°C below the surface temperature. In panel (c), oxygen contours 75 and 150 μmol L^{-1} are indicated in black to highlight the high surface concentration that is not shown by the color scale, and contour 1 μmol L^{-1} is indicated in white. The boundaries between adjacent transects are indicated by black vertical lines and the transect number as $T_{1–4}$.

3.2. Mesoscale and Submesoscale Circulation

3.2.1. Eddy Dynamics

The surface signature of the two anticyclonic eddies traversed by the ship track can be detected as a positive anomaly on altimetry maps (Figure 1a). The southern eddy (Papagayo eddy, Figure 1) is first detected on satellite sea level maps on 4 August 2021 in the Gulf of Papagayo (10.3°N, 86.4°W). However, it does not begin detaching from the coast until early December. From there, the eddy starts traveling west and decays on 3 February 2023 at 94.6°W (900 km from its formation site) exhibiting a SLA of ∼35 cm. The northern eddy (Tehuantepec eddy, Figure 1) appears first on the mesoscale eddy trajectory atlas on 1 December 2021 at 13.4°N/79.9°W, but the SLA (∼40 cm) can be detected as early as October 1st in the northern part of the Gulf of Tehuantepec. During this period, particularly strong winds have been observed in the Gulf of Tehuantepec reaching velocities above 15 m s^{-1} during November 2021 (Figure 5a). This eddy travels significantly further west, reaching 120.1°W (∼2,600 km from its region of formation) before decaying on 11 October 2022.

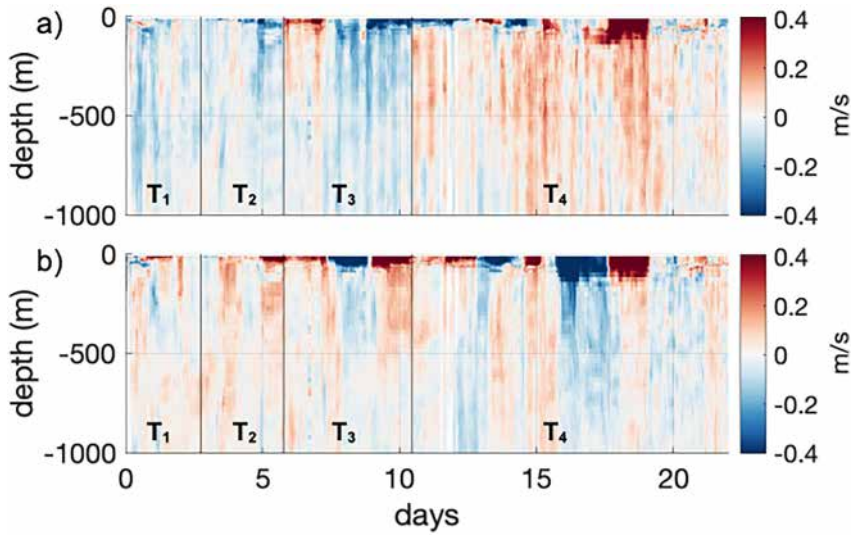

Figure 4. Vertical sections of (a) zonal and (b) meridional velocity (m s^{-1}) measured using acoustic doppler current profilers along the ship's track. Days are counted from 23 December 2021. Vertical lines indicate the boundaries between transects.

Acoustic doppler current profilers data along the ship's trajectory reveal that the Papagayo eddy has a maximum swirl velocity of ∼0.7 m s^{-1} and a diameter, calculated as the distance between the two velocity maxima, of ∼265 km (Figure 4). The Tehuantepec eddy has a diameter of ∼335 km and a maximum velocity of ∼1.25 m s^{-1} at the time of the ship's crossing (Figure 4).

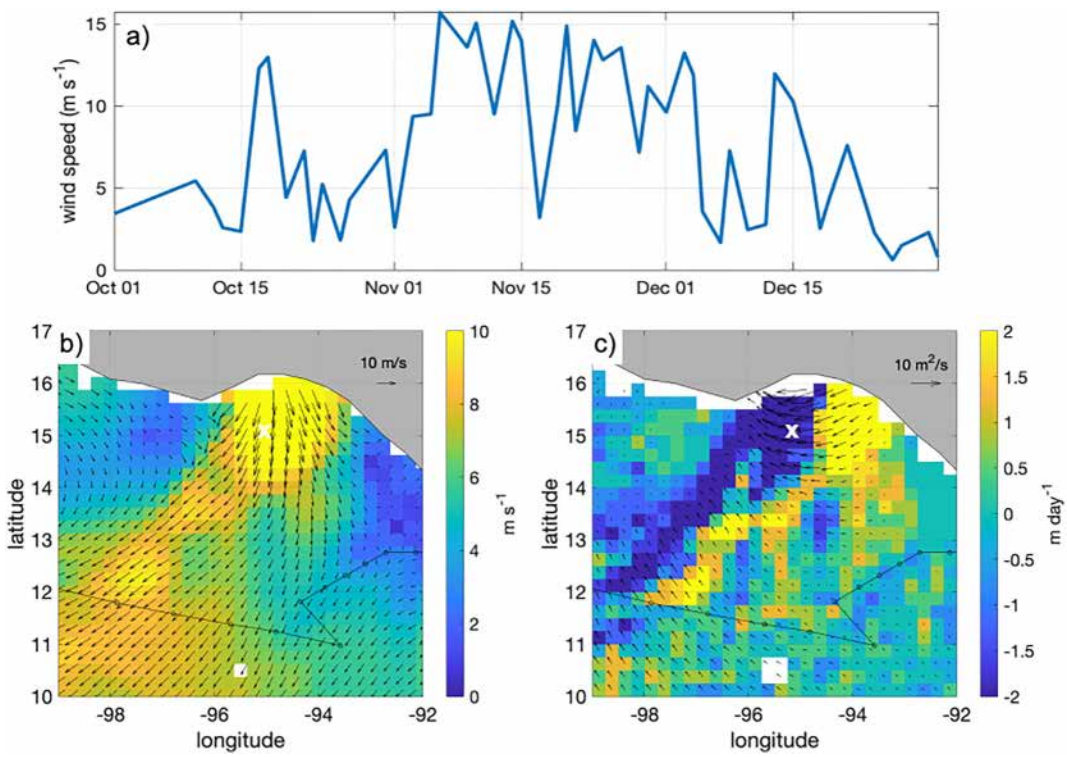

Figure 5. (a) Wind speed in the Gulf of Tehuantepec from 1st October to 31st December 2021; the time series correspond to the data at the position of the white cross on panels (b) and (c). (b) Wind speed at 10 m superimposed with wind vectors and (c) Ekman pumping superimposed with Ekman transport vectors for 3 December 2021. The ship's track is indicated in black with the stations highlighted by black dots.

As observed from CTD casts (Figure 3), both anticyclones exhibit core water mass properties that are warmer and fresher than the exterior hydrographic properties. Relatively intense horizontal density gradients can be observed at the edges. A deepening of the oxycline is apparent inside both eddies; the region of a high vertical gradient of dissolved oxygen located at ∼50 m depth on the eddies edges reaches ∼100 m depth in the eddies centers. The centers of the eddies are also characterized by low chlorophyll fluorescence (Figure 2) while the edges exhibit high chlorophyll filaments. A deep chlorophyll maximum that connects to the high surface fluorescence on the rim can be observed in both eddies around 50 m depth (Figure 3).

3.2.2. Stirring of the Biogeochemical Fields

Satellite maps of chl-a reveal high concentration areas organized in submesoscale patterns. Elongated filaments originating in both Gulfs and extending offshore can be observed around the time of SR2114 (Figure 2). Of particular interest is a filamentary structure originating at the coast, specifically in the north of the Gulf of Tehuantepec, extending offshore and meandering along the rim of the large anticyclonic eddy observed on the fourth transect of the campaign. This filament exhibits elevated chlorophyll levels visible on satellite maps (Figures 2a and 2b) that align with Lyapunov exponents minima (high negative values) suggesting a high stirring region. The coastal portion of the filament closely follows the path of the high wind region observed on satellite maps (Figure 5b). Indeed in this part of the Gulf, a gap in the mountain range allows the passage of 'gap winds' (Figure 2), which are intense and intermittent wind jets that can drive upwelling on their left flank. Where, positive wind stress curl is expected to enhance nutrient supply locally through Ekman pumping. As such, the high chlorophyll concentration in and outside the Gulf suggests that upwelling processes could bring nutrient-rich waters to the surface, fueling phytoplankton growth. The high chlorophyll water is then advected offshore along the filament eventually wrapping itself around the periphery of an anticyclonic eddy. These observations suggest that the surface chl-a patterns are closely linked to the combined effects of wind forcing and local current dynamics, including mesoscale and submesoscale stirring.

Importantly, the evolution of the Tehuantepec eddy appears to influence these biogeochemical patterns. Between December 1st and 15th, when the eddy was located near the coast and likely in an intensifying phase, elevated chlorophyll concentrations were observed along its rim (Figures 2a and 2b). By January 1st and 15th, as the eddy moved offshore and matured, chlorophyll concentrations decreased significantly (Figures 2c and 2d). This pattern points to a potential coupling between the eddy life cycle and biological productivity, whereby coastal upwelling and offshore transport are more effective during the early stages of eddy development. Wind-eddy interactions may also enhance vertical nutrient fluxes at the eddy's periphery during this phase, reinforcing biological responses.

Local production within the filament could also play a role in the observed chl-a concentration as the interplay of submesoscale and mesoscale circulation could drive frontal processes and associated vertical fluxes. In fact, Ekman pumping, which represents the wind stress curl-driven vertical velocity at the base of the Ekman layer, shows positive velocities along the filament structure that extend almost to the ship's tracks (Figure 5c), underscoring the wind's role in sustaining surface productivity.

Another second filament of high chlorophyll concentration can be observed south of the Gulf of Papagayo, where similar gap wind dynamics are at play (Figure 2). This filament similarly wraps itself around the corresponding Papagayo eddy, reinforcing the idea that episodic wind forcing and eddy-wind interactions jointly shape the offshore distribution of biological activity in the ETNP.

A subsurface oxygen maximum (SOM) is another prominent characteristic that appears to be linked to the mesoscale and submesoscale dynamics of the ETNP (Figure 3). Located on the outskirts of the ODZ, the Papagayo eddy resides within a region of elevated oxygen levels. As such, the higher oxygen concentration observed at depth on the eastern flank of the eddy likely originates from the adjacent coastal maximum (Figure 3c). In contrast, the Tehuantepec eddy is observed passing through an oxygen-depleted area, with dissolved oxygen concentrations falling below 1 μmol L^{-1} at depths beyond 100 m. However, despite the low-oxygen conditions, several ship stations surrounding the eddy reveal a localized relative maximum (over 5 μmol L^{-1}) centered on the isopycnal 26.4, spanning depths of 150–250 m (Figures 6a and 6b). This SOM is also observed in one of the two floats that circle around the eddy (Figures 6 and 7). On the southern flank of the eddy, higher concentrations of oxygen can be detected at the depth of the isopycnal 26.5 (Figures 6d and 7b), while on the northern flank of the eddy, the waters remain anoxic (Figures 6c and 7a). The sporadic distribution of the SOM

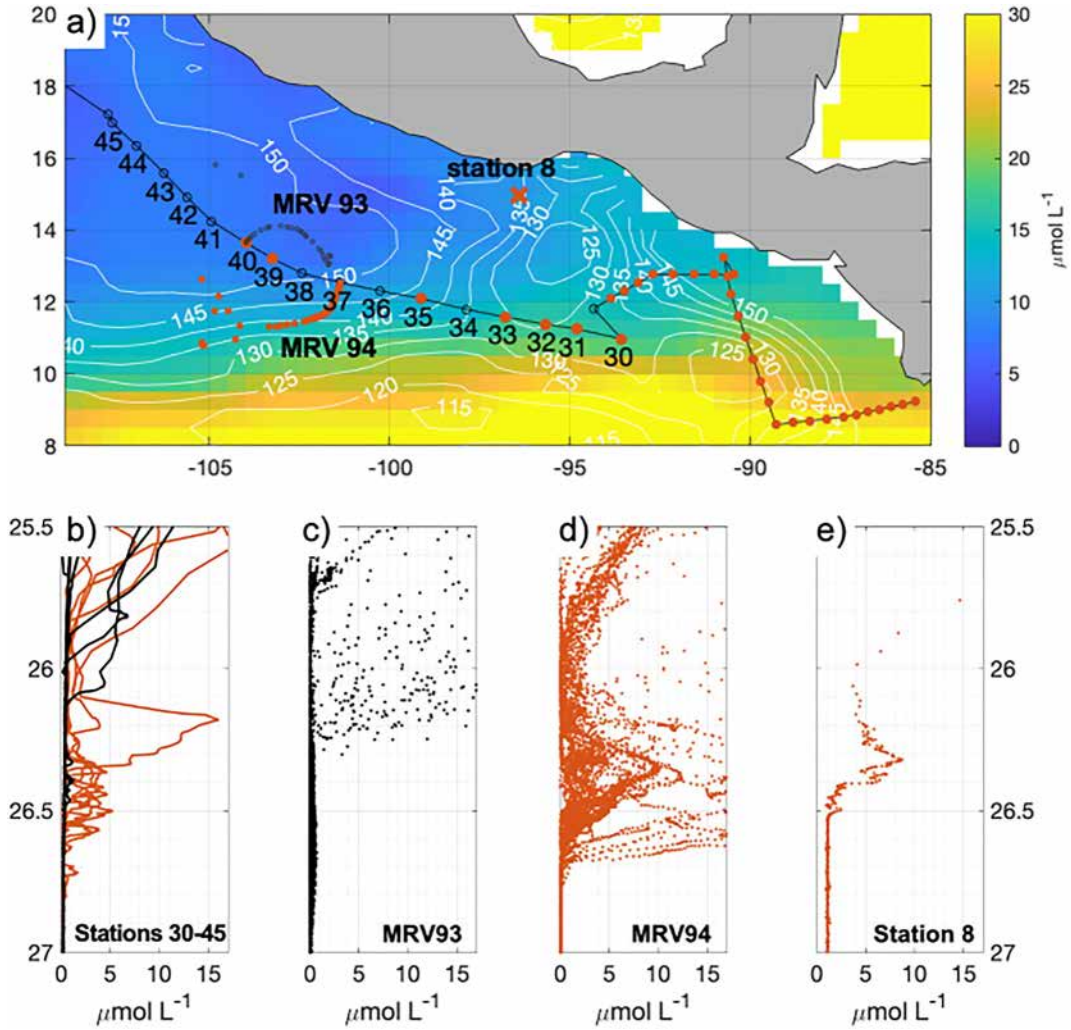

Figure 6. (a) Climatology of dissolved oxygen concentration from Roach and Bindoff (2023, μmol L^{-1}) along isopycnal 26.4. White contours represent the depth of the isopycnal surface. The ship's track, as well as the floats trajectories and the location of station 8, is overlaid in black. The positions of the profiles exhibiting a subsurface oxygen maxima (SOM) are highlighted in orange. Vertical profiles of dissolved oxygen recorded (b) at ship's stations 30 to 45, (c) by float 93, (d) float 94, and (e) at station 8. Orange color indicates the observation of an SOM.

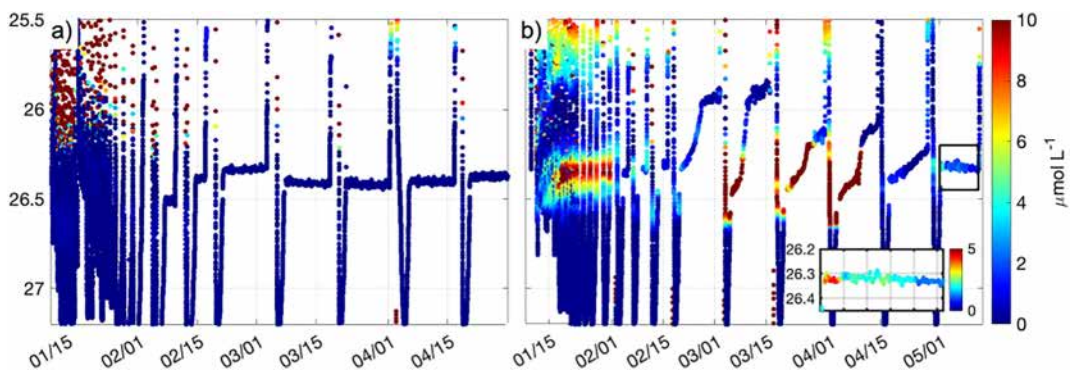

Figure 7. Dissolved oxygen concentration observed by (a) float 93 and (b) float 94. The inset in panel (b) is a detail of one of the float drift that is highlighted by the black square on the figure.

raises questions about its origins and the underlying physical and biogeochemical dynamics. Note that similar oxygen values were observed on isopycnal 26.4 close to the coast in the Gulf of Tehuantepec, in February 2023 at station 8 (Figure 6e), at the same density range. To better understand the transport pathways and unravel the role of different oceanic features in shaping these observed distributions, an integrated approach, based on particle tracking, is outlined in the following section.

3.3. Lagrangian Analysis of the Water Parcels

3.3.1. Surface Backtracking

A particle tracking algorithm was used to elucidate the pathways and transport mechanisms governing the distribution of the biogeochemical fields. Understanding the origins of features such as surface chlorophyll filaments and subsurface higher oxygen concentrations reaching the ODZ within this complex oceanic environment is essential for unraveling the mechanisms driving biological productivity and oxygen dynamics.

The first numerical experiment was conducted using satellite-derived surface geostrophic velocities. Particles were initially placed every 30 km along the ship track for a total of 110. These particles were then tracked backward in time for 120 days providing insights into the trajectories and origins of the surface features observed during the campaign. Analysis of the particle trajectories reveals diverse transport pathways and origins. Surface water masses observed during the first two transects mostly originate from the equatorial current system (orange dots in Figure 8a), indicating long-range transport from equatorial regions, probably along the NECC, before entering the CRD region. This is coherent with the horizontal currents observed on the ADCP vertical sections (Figure 3). Northward, a few localized regions contain water parcels that originated from the north (cyan dots in Figure 8a); however, a significant proportion of particles remained within the coastal region for the entire 120-day period (black dots, Figure 8a).

Selected trajectories in and around both eddies illustrate how particles have traveled in the area. The Papagayo eddy is formed of a mix of water from the Gulf of Papagayo and from the equatorial current system, while most of the Tehuantepec eddy water parcels and surrounding waters originate from the coastal area in and around the Gulf of Tehuantepec and have been advected and stirred by the mesoscale field for several months. Note that a number of particles inside the Tehuantepec eddy have followed a trajectory corresponding to the high chlorophyll filament structure.

In order to assess the accuracy and reliability of HYCOM's representation of horizontal current, the backward tracking experiment is reproduced using HYCOM horizontal velocities vertically averaged over the upper 20 m of the water column in order to temper the wind-driven surface turbulent velocity (Figure 8b). By comparing the simulated particle trajectories with those obtained from satellite-based velocities, we can evaluate the model's ability to accurately represent surface current patterns and transport pathways in the ETNP. Note that HYCOM's surface velocity also includes wind-driven Ekman currents. Both experiments show similar patterns (Figure 8), with southern particles coming from the equatorial current system and northern particles coming from an equatorward coastal current, albeit a higher number of parcels are coming from the north driven by HYCOM's velocities. The eddy dynamics is also well reproduced with both eddies signatures clearly visible in particle pathways. Overall HYCOM advection patterns seem more energetic and particles tend to travel faster in the simulation, which can be due to the wind-driven transport, but the dominant flow patterns and transport pathways are accurately captured. This agreement provides confidence in the model's ability to simulate advection dynamics in the ETNP.

These results provide evidence of the complex mechanisms governing the transport pathways of surface features in the ETNP. Water masses transported from distant regions by the NECC in the south and the California Current in the north become trapped within the coastal region for an extended period. They undergo stirring and mixing induced by the mesoscale field and strong localized gap winds, leading to the development of fine-scale structures.

While the surface analysis provides valuable insights into advective processes and surface dynamics, it remains unclear whether these processes extend into the subsurface. Specifically, the sporadic distribution of the subsurface relative oxygen maximum (Figure 6) presents an intriguing phenomenon with the potential to oxygenate anoxic ODZ waters. To elucidate the dynamics driving these subsurface features, we transition to an investigation of the 3D oceanic environment using a numerical model of the region.

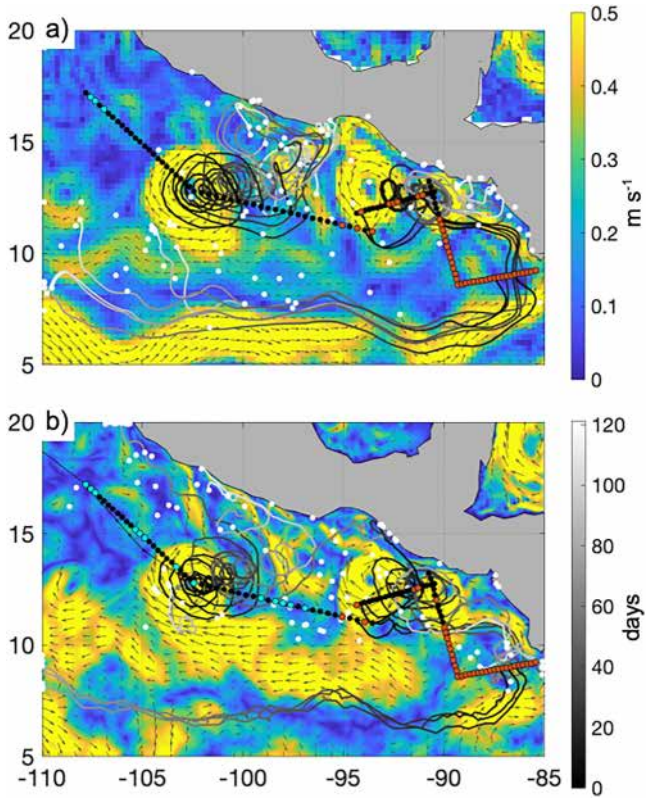

Figure 8. (a) Satellite geostrophic velocity (ms^{-1}) and (b) horizontal velocity (ms^{-1}) averaged between the surface and 20 m depth derived from the HYCOM hindcast for 10 January 2022. The arrows represent the direction of the flow. The dots along the ship's tracks represent the initial particle positions prior to the backtracking. The particle positions 120 days prior is shown in white. In orange are the particles that originate in equatorial waters, defined here as any particle that reaches a position south of 6°N. Particles that originate from the north (north of 19°N) are shown in cyan, and particles that remained within those latitudes are shown in black. The lines represent select trajectories and the black to white gradient the time elapsed.

3.3.2. Subsurface Advection of Particles

HYCOM's performance in reproducing subsurface current structure and variability is assessed by comparing the model to in situ ADCP measurements collected along the fourth section, parallel to the coast of Mexico (Figure 9). Zonal (v) velocities show good correspondence in terms of spatial distribution and magnitude. The eddy structure is well reproduced by the model at the correct location and with the same width even though the structure is more energetic and larger velocities are observed at greater depth. The surrounding velocities also show similarities except on the west side of the eddy (106–105°W) where model-computed velocities are positive and observed velocities are negative in the surface layer and on the east side (100–99°W, 0–50 m depth) where positive velocities are not captured by the model. Generally, the good agreement between the model simulation and observational data indicate the model's ability to capture the dynamics of the ETNP in particular around the depth and density where the oxygen intrusions have been observed (150–250 m depth and $\sigma_\theta \sim 26.4$ kg m^{-3}).

A second tracking experiment was then performed using HYCOM subsurface horizontal velocities in order to assess the distribution of particles originating from the coast on isopycnal 26.4. First, horizontal velocities from the model were interpolated over the density layer 26.4, where the intrusions of high dissolved oxygen concentrations have been observed. Then, particles were released along the entire coastline of the ETNP and tracked forward in time. Although HYCOM accurately represents broad-scale circulation, it may not precisely capture fine-scale features and short-term variability. Therefore, instead of tracking backward water masses at the exact locations of the observed intrusions, we investigate pathways from the coast into the ODZ. Such a particle tracking experiment offers the opportunity to investigate the overarching circulation patterns and understand the general pathways from the coast into the ODZ despite potential discrepancies in small-scale variability.

Every day from 1st September to 30th September 2021, a total of 95 particles were introduced along the entire coastline of the ETNP at 20 km intervals, spanning from 9.8 to 17°N along the density surface 26.4 (Figure 10). This spatial coverage allows for a thorough investigation of the pathways leading into the ODZ and the coastal retention mechanisms influencing subsurface dynamics. The 2,850 released particles in total were then tracked forward in time for 4 months (120 days) using the interpolated HYCOM velocities on isopycnal 26.4.

At the end of the tracking period (Figure 10c), some particles are still retained inside the Gulf of Tehuantepec, but most of them have traveled offshore along filamentary structures. Particles originating from the northern and central part of the Gulf of Tehuantepec travel the furthest into the ODZ (highlighted with their trajectory printed on Figure 10). This region was also identified by the previous backtracking experiment as the source of the surface water above the relatively oxygenated water parcels observed during the cruise. Additionally, those particles travel offshore following the direction of intense winds (Figure 5), similar to what was observed for the surface filament, some of them showing signs of being trapped inside the westward drifting eddy. In general, the particles are distributed along elongated filaments, with a tendency to follow the direction of wind jets emanating from both the Gulfs. These findings underscore the importance of small-scale processes and filamentation in shaping subsurface circulation patterns within the ETNP. Moreover, the influence of wind jets on particle trajectories is evident even at depths of 150–250 m, corresponding to the depth range of the isopycnal 26.4.

4. Discussion and Conclusions

Our study investigates the interplay between the mesoscale and submesoscale circulations in the ODZ of the ENTP and their influence on biogeochemical distributions. Surface satellite data reveal dynamic chlorophyll

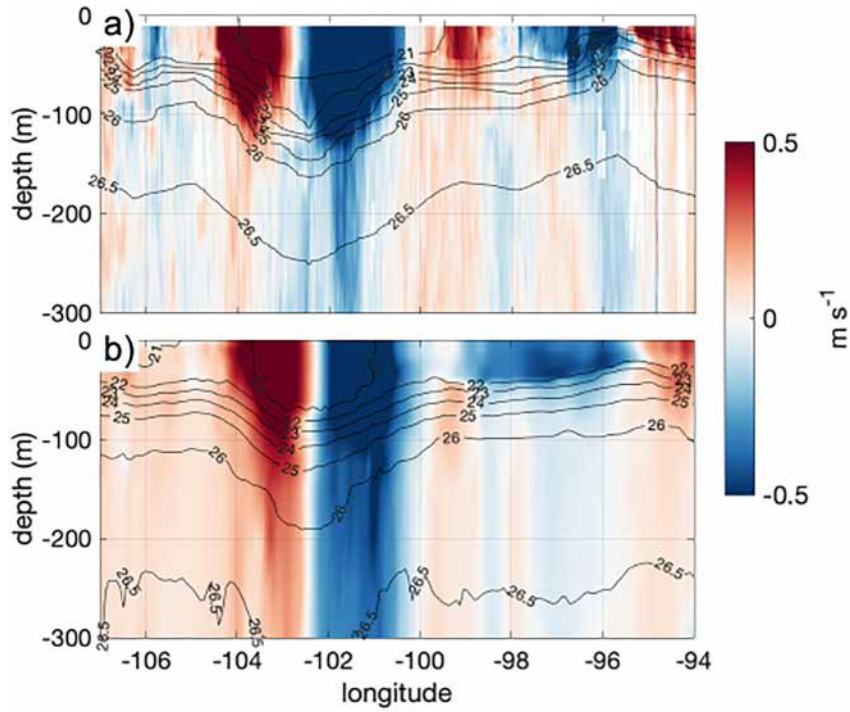

Figure 9. Vertical sections of horizontal zonal velocity (a) measured using the onboard acoustic doppler current profilers between 3 and 14 January 2022 and (b) derived from the HYCOM model simulation along the fourth transect on January 10.

filaments originating from two important gulfs where strong gap winds drive coastal upwelling and propel water masses offshore along mesoscale eddies and elongated filaments. These features coincide with regions of high FSLE, indicating intense stirring and mixing processes.

Two mesoscale eddies exhibiting distinct biogeochemical signatures were observed during the time of the cruise: The Papagayo eddy, situated near the ODZ boundary, showcases elevated oxygen levels likely advected from the coastal region and the Tehuantepec eddy that traverses an oxygen-depleted zone but still manifests localized oxygen maxima at depth, suggesting complex subsurface dynamics.

The influence of small-scale processes and filamentation on the distribution of biogeochemical properties is evident from our analysis. The surface chl-a data show filaments originating from the coast, traveling offshore along regions of high wind jets, and displaying submesoscale patterns. These filaments are areas of high stirring, as suggested by the FSLE maxima. This stirring likely plays a crucial role in the distribution of biogeochemical properties, such as oxygen and chl-a, by enhancing mixing and transport processes.

The sporadic oxygenated patches within the ODZ at around 150–250 m depth on the isopycnal 26.4 raise intriguing questions about subsurface processes. This SOM, observed intermittently along the ship's transect and a float trajectory, does not perfectly align with surface chlorophyll distributions, indicating the presence of complex subsurface dynamics. Particle tracking experiments, conducted using both observational data and HYCOM model simulations, trace these oxygenated waters back to coastal origins. In particular, the northern and central regions of the Gulf of Tehuantepec seem to host the water parcels that travel further west inside the ODZ core. Coastal observations from February 2023 reveal the presence of the same SOM at density levels 26.2–26.4, confirming that waters just north of the Gulf of Tehuantepec can also exhibit these oxygenated subsurface layers.

The question of how this subsurface layer becomes oxygenated, despite not directly reaching the surface, remains central to understanding the dynamics of the region. It can result either from horizontal advection of water from a region with higher oxygen concentrations or from vertical mixing with the more oxygenated surface layer. Considering the general distribution of oxygen in the region, the first hypothesis implies a northern transport of water along the coast between the Gulf of Papagayo and the Gulf of Tehuantepec. The second hypothesis suggests the action of the gap winds in mixing the coastal waters.

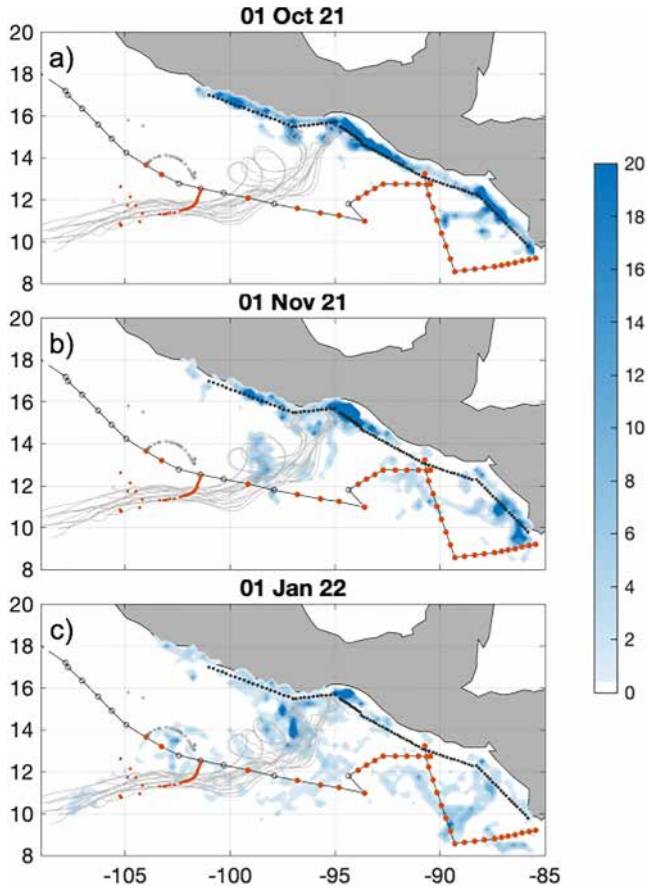

Figure 10. Distribution of particles released along the coast and advected over isopycnal 26.4 by HYCOM-simulated horizontal velocities on (a) 01 October 2021, (b) 01 November 2021, and (c) 01 January 2022. Shades of blue indicate the particle count for every 0.25° grid cell, and the black dots the release location of the particles. Selected trajectories plotted in gray represent the particles traveling further west. The ship's track, stations, and floats trajectories are indicated in dark gray; stations showing a subsurface oxygen maximum are highlighted in orange.

We showed that coastal wind jets, particularly in the Gulf of Tehuantepec, can drive intense horizontal transport of the surface layer and upward and downward vertical velocities through Ekman dynamics (Figure 5c). In fact, previous studies have demonstrated that the cold water tongue generated by wind-driven upwelling can reach temperatures as low as 14°C at the surface during winter (Barton et al., 2009). This significant cooling indicates that the 26.4 isopycnal, which corresponds roughly to 13°C temperature, could be brought into contact with surface waters, allowing it to become oxygenated near the coast. The strong wind jets, which blow through mountain gaps, not only drive upwelling but also enhance vertical mixing, facilitating the oxygenation of these deeper waters before they are subducted and transported offshore as part of the regional circulation. This particularly highlights the significant influence of wind jets on subsurface layers.

The fact that the wind jets originating near the Gulf of Tehuantepec drive vertical structures that extend well below the expected Ekman layer depth, reaching down to the 26.4 isopycnal surface (~150–200 m depth) also suggests that processes beyond classical wind-driven Ekman transport could be at play. One possible mechanism is the interaction between wind forcing and mesoscale eddies, which are numerous in the region and can modulate the biogeochemical activity (Figure 2). In regions of strong wind stress curl anomalies, such as those induced by orographic wind jets, vertical and lateral transport can be enhanced by eddy-wind coupling (Chelton et al., 2011; Gaube et al., 2014). These interactions can strengthen the vertical coherence of eddies, facilitating the offshore transport of subsurface water masses. Such mechanisms likely contribute to the offshore ventilation of the ODZ interior and may help explain the depth and persistence of the SOM observed in our data.

In addition to physical processes, biogeochemical activity is also certainly at play in shaping the observed data. In particular, the MRV floats were programmed to track along specific density layers during their deployment to observe the oxygen variability. The inset in Figure 7b shows one of the drifts around density layer 26.4. The oxygen concentration shows a peak of 5 μmol L^{-1} that decreases to 1 μmol L^{-1} over about 10 days, which could be indicative of respiration taking place (Altabet et al., in prep). This implies regeneration of NH4+ from organic matter diagenesis that would fuel anammox removal of biologically available nitrogen once sufficiently low O_2 was achieved.

Besides providing information on the origin of the SOM, the particle tracking experiments also revealed distinct pathways for water parcels inside the ODZ depending on their location. South of approximately 14°N, water parcels are predominantly advected from the south and in particular, from the equatorial current system. In contrast, north of 14°N, water parcels primarily originate from the northern coastal regions or directly from the coast where they have a long residency time. This demarcation has significant implications for understanding the spatial variability in the ODZ properties since water parcels of different origin likely carry different nutrient loads and oxygen concentrations.

The integrated approach using both observational data and particle tracking experiments has provided valuable insights into the dynamics of the ETNP. The differentiation in water parcel origins, the influence of wind jets, and the role of small-scale processes all contribute to the complex biogeochemical environment observed in this region. Our findings underscore the importance of considering both large-scale currents and small-scale processes for comprehending the biogeochemical distribution of properties in the ETNP. The sporadic distribution of SOM and its relation to surface filamentary structures suggest complex interactions between physical and biogeochemical processes that warrant further investigation. Despite the robust insights gained, our study faces limitations, including the temporal and spatial resolution of observational data. The detailed mechanisms driving the

observed oxygen intrusions still remain partially elusive, warranting further investigation. Understanding these dynamics is crucial for predicting nutrient cycling, primary productivity, and the potential impact of climate change on marine ecosystems. Future research should aim to refine these aspects and explore the temporal variability of these processes to provide a more comprehensive understanding of the region's biogeochemical dynamics.

Data Availability Statement

This study has been conducted using several Copernicus Marine Environment Monitoring Service (CMEMS, http://marine.copernicus.eu) data sets. In particular, the SLA and surface geostrophic velocities are detailed and available for download at https://data.marine.copernicus.eu/product/SEALEVEL_GLO_PHY_L4_MY_008_047/description (https://doi.org/10.48670/moi-00148), the ocean color data at https://data.marine.copernicus.eu/product/OCEANCOLOUR_GLO_BGC_L3_NRT_009_101/description (https://doi.org/10.48670/moi-00282), and the wind data at https://data.marine.copernicus.eu/product/WIND_GLO_PHY_L3_NRT_012_002/description. Two value-added products developed by the Archiving, Validation, and Interpretation of Satellite Oceanographic (AVISO) service are supporting our analysis, the finite-size Lyapunov exponents (FSLE, https://www.aviso.altimetry.fr/en/data/products/value-added-products/fsle-finite-size-lyapunov-exponents.html, https://aslopubs.onlinelibrary.wiley.com/doi/full/10.1002/lno.12654) and the Mesoscale Eddy Trajectories Atlas (META3.2 DT, https://www.aviso.altimetry.fr/en/data/products/value-added-products/global-mesoscale-eddy-trajectory-product.html, https://link.springer.com/article/10.1007/s13131-023-2278-3). The global oxygen Atlas (Roach & Bindoff, 2023, https://doi.org/10.1175/JTECH-D-23-0007.1) is available at https://researchdata.edu.au/roach-bindoff-global-2018-v10/2759451. The Sally Ride cruise data SR2114 are available at https://www.rvdata.us/search/cruise/SR2114 (https://www.bco-dmo.org/deployment/931391) and the MRV floats data at https://datadryad.org/dataset/doi:10.5061/dryad.8kprr4xwk.

Acknowledgments
We would like to thank C. Buckingham and A. Tandon for their valuable discussions during the preparation of this paper. We also appreciate the support of the RV Sally Ride crew during the cruise. Financial support came from US NSF Grant#1851361 and US ONR Grants# N00014-20-1-2849.

References

Barton, E. D., Lavín, M. F., & Trasviña, A. (2009). Coastal circulation and hydrography in the Gulf of Tehuantepec, Mexico, during winter. *Continental Shelf Research*, *29*(2), 485–500. https://doi.org/10.1016/j.csr.2008.12.003

Chelton, D. B., Schlax, M. G., & Samelson, R. M. (2011). Global observations of nonlinear mesoscale eddies. *Progress in Oceanography*, *91*(2), 167–216. https://doi.org/10.1016/j.pocean.2011.01.002

Dämmer, L. K., de Nooijer, L., van Sebille, E., Haak, J. G., & Reichart, G.-J. (2020). Evaluation of oxygen isotopes and trace elements in planktonic foraminifera from the Mediterranean Sea as recorders of seawater oxygen isotopes and salinity. *Climate of the Past*, *16*(6), 2401–2414. https://doi.org/10.5194/cp-16-2401-2020

d'Ovidio, F., Fernández, V., Hernández-García, E., & López, C. (2004). Mixing structures in the mediterranean sea from finite-size Lyapunov exponents. *Geophysical Research Letters*, *31*(17), L17203. https://doi.org/10.1029/2004gl020328

Duncan, E. M., Arrowsmith, J., Bain, C., Broderick, A. C., Lee, J., Metcalfe, K., et al. (2018). The true depth of the Mediterranean plastic problem: Extreme microplastic pollution on marine turtle nesting beaches in Cyprus. *Marine Pollution Bulletin*, *136*, 334–340. https://doi.org/10.1016/j.marpolbul.2018.09.019

Duteil, O., Schwarzkopf, F. U., Böning, C. W., & Oschlies, A. (2014). Major role of the equatorial current system in setting oxygen levels in the eastern tropical Atlantic ocean: A high-resolution model study. *Geophysical Research Letters*, *41*(6), 2033–2040. https://doi.org/10.1002/2013gl058888

Engel, A., Kiko, R., & Dengler, M. (2022). Organic matter supply and utilization in oxygen minimum zones. *Annual Review of Marine Science*, *14*, 355–378. https://doi.org/10.1146/annurevmarine-041921-090849

Fiedler, P. C., Mendelssohn, R., Palacios, D. M., & Bograd, S. J. (2013). Pycnocline variations in the eastern tropical and north pacific, 1958-2008. *Journal of Climate*, *26*(2), 583–599. https://doi.org/10.1175/JCLI-D-11-00728.1

Firing, E., Ranada, J., & Caldwell, P. (1995). *Processing ADCP data with the CODAS software system version 3.1*. Joint Institute for Marine and Atmospheric Research, University of Hawaii and National Oceanographic Data Center. https://epic.awi.de/id/eprint/29904/1/Fir1995b.pdf

Gangrade, S., & Franks, P. J. S. (2023). Phytoplankton patches at oceanic fronts are linked to coastal upwelling pulses: Observations and implications in the California Current System. *Journal of Geophysical Research: Oceans*, *128*(3), e2022JC019095. https://doi.org/10.1029/2022JC019095

Gaube, P., McGillicuddy, D. J., Jr., Chelton, D. B., Behrenfeld, M. J., & Strutton, P. G. (2014). Regional variations in the influence of mesoscale eddies on near-surface chlorophyll. *Journal of Geophysical Research: Oceans*, *119*(12), 8195–8220. https://doi.org/10.1002/2014JC010111

Hasson, A., Farrar, J. T., Boutin, J., Bingham, F., & Lee, T. (2019). Intraseasonal variability of surface salinity in the eastern tropical pacific associated with mesoscale eddies. *Journal of Geophysical Research: Oceans*, *124*(4), 2861–2875. https://doi.org/10.1029/2018JC014175

Kessler, W. S. (2006). The circulation of the eastern tropical pacific: A review. *Progress in Oceanography*, *69*(2), 181–217. https://doi.org/10.1016/j.pocean.2006.03.009

Kwiecinski, J. V., & Babbin, A. R. (2021). A high-resolution atlas of the eastern tropical pacific oxygen deficient zones. *Global Biogeochemical Cycles*, *35*(12), e2021GB007001. https://doi.org/10.1029/2021GB007001

Lange, M., & van Sebille, E. (2017). Parcels v0.9: Prototyping a Lagrangian ocean analysis framework for the petascale age. *Geoscientific Model Development*, *10*(11), 4175–4186. https://doi.org/10.5194/gmd-10-4175-2017

Lévy, M., Franks, P. J. S., & Smith, K. S. (2018). The role of submesoscale currents in structuring marine ecosystems. *Nature Communications*, *9*(1), 4758. https://doi.org/10.1038/s41467-018-07059-3

Margolskee, A., Frenzel, H., Emerson, S., & Deutsch, C. (2019). Ventilation pathways for the North pacific oxygen deficient zone. *Global Biogeochemical Cycles*, *33*(7), 875–890. https://doi.org/10.1029/2018GB006149

McNeil, C. L., D'Asaro, E. A., Altabet, M. A., Hamme, R. C., & Garcia-Robledo, E. (2023). Autonomous observations of biogenic N2 in the Eastern Tropical North Pacific using profiling floats equipped with gas tension devices. *Frontiers in Marine Science*, *10*(June), 1–15. https://doi.org/10.3389/fmars.2023.1134851

Nagai, T., Gruber, N., Frenzel, H., Lachkar, Z., McWilliams, J. C., & Plattner, G.-K. (2015). Dominant role of eddies and filaments in the offshore transport of carbon and nutrients in the California Current System. *Journal of Geophysical Research: Oceans*, 2813–2825. https://doi.org/10.1002/2015JC010889.Received

Oschlies, A., Brandt, P., Stramma, L., & Schmidtko, S. (2018). Drivers and mechanisms of ocean deoxygenation. *Nature Geoscience*, *11*(7), 467–473. https://doi.org/10.1038/s41561-018-0152-2

Pegliasco, C., Delepoulle, A., Mason, E., Morrow, R., Faugère, Y., & Dibarboure, G. (2022). META3.1exp: A new global mesoscale eddy trajectory atlas derived from altimetry. *Earth System Science Data*, *14*(3), 1087–1107. https://doi.org/10.5194/essd-14-1087-2022

Revsbech, N. P., Thamdrup, B., Dalsgaard, T., & Canfield, D. E. (2011). Construction of STOX oxygen sensors and their application for determination of O_2 concentrations in oxygen minimum zones. *Methods in Enzymology*, *486*, 325–341. https://doi.org/10.1016/b978-0-12-381294-0.00014-6

Roach, C. J., & Bindoff, N. L. (2023). Developing a new oxygen atlas of the world's oceans using data interpolating variational analysis. *Journal of Atmospheric and Oceanic Technology*, *40*(11), 1475–1491. https://doi.org/10.1175/JTECH-D-23-0007.1

Schilling, H. T., Everett, J. D., Smith, J. A., Stewart, J., Hughes, J. M., Roughan, M., et al. (2020). Multiple spawning events promote increased larval dispersal of a predatory fish in a western boundary current. *Fisheries Oceanography*, *29*(4), 309–323. https://doi.org/10.1111/fog.12473

Schmidtko, S., Stramma, L., & Visbeck, M. (2017). Decline in global oceanic oxygen content during the past five decades. *Nature*, *542*(7641), 335–339. https://doi.org/10.1038/nature21399

Willett, C. S., Leben, R. R., & Lavin, M. F. (2006). Eddies and tropical instability waves in the eastern tropical pacific: A review. *Progress in Oceanography*, *69*(2–4), 218–238. https://doi.org/10.1016/j.pocean.2006.03.010